Advances in Aircraft and Spacecraft Science, *Vol. 10, No. 2 (2023) 127-140*
https://doi.org/10.12989/aas.2023.10.2.127

Thermoelastic deformation behavior of functionally graded cylindrical panels with multiple perforations

Shyam K. Chaudhary[1a], Vishesh R. Kar*[1] and Karunesh K. Shukla[2b]

[1]*Department of Mechanical Engineering, National Institute of Technology Jamshedpur, 831014, India*
[2]*Department of Civil Engineering, National Institute of Technology Jamshedpur, 831014, India*

(Received October 5, 2022, Revised January 4, 2023, Accepted January 5, 2023)

Abstract. The present article focuses on the thermoelastic deformation behavior of inhomogeneous functionally graded metal/ceramic cylindrical shell structure with multiple perforations using 2D finite element approximation. Here, cylindrical shell structure is considered with single (1×1) and multiple (2×2, 3×3 and 4×4) perforations. The temperature-dependent elastic and thermal properties of functionally graded material are evaluated using Voigt's micromechanical material scheme via power-law function. The kinematics of the proposed model is based on the equivalent single-layer first-order shear deformation mid-plane theory with five degrees-of-freedom. Here, 2D isoparametric finite element solutions are obtained using eight-node quadrilateral elements. The mesh refinement of present finite element model is performed to confirm the appropriate number of elements and nodes for the analysis purpose. Subsequently, a comparison test is conducted to demonstrate the accuracy of present results. In later section, numerous numerical illustrations are demonstrated at different set of conditions by varying structural, material and loading parameters and that confirms the significance of various parameters such as power-law index, aspect ratio, thickness ratio, curvature ratio, number of perforations and temperature on the deformation characteristics of functionally graded cylindrical shell structure.

Keywords: 2D-FEM; cylindrical; deformation; FGM; perforations; temperature-dependent; thermoelastic

1. Introduction

Advanced composites are being utilized in various engineering sectors, such as spacecraft, energy, automobile, aerospace, etc., due to their high specific strength. It is evident that conventional laminated composites cannot survive under unlike environmental conditions and mostly experience delamination phenomenon. In this regard, functionally graded materials (FGMs) have drawn attention in various engineering sectors due to their customized properties. In FGMs, material properties vary gradually in spatial direction, typically in thickness of the panel, between metal-rich to ceramic-rich (Birman and Byrd 2007). The gradual variation results in a very efficient material tailored to meet the requirement of high-performance structures/components operating in extreme conditions. The use of perforated structures in various engineering sectors are being predominant due to their lightweight, high heat-dissipation rate and other ergonomic/aesthetic design requirements. These types of structural components are mostly

*Corresponding author, Ph.D., E-mail: kumarshyam72@gmail.com
[a]Professor, E-mail: visheshkar@gmail.com

http://www.techno-press.org/?journal=aas&subpage=7 ISSN: 2287-528X (Print), 2287-5271 (Online)

utilised in filters, disc brakes, ventilated casings, automobile silencer, embossed floors in ships, etc.

Therefore, it is vital to examine high-performance structures/components made of FGM with perforations under hostile environmental conditions. Due to complexity and expensiveness in synthesis and testing, most of the reported researches on this type of material/structure are limited to theoretical examinations. The modelling and analysis of functionally graded (FG) structures has been continued from last two decades to come up with the new/modified mathematical model and solution techniques to overcome the drawbacks of the former studies (Birman and Byrd 2007, Liew *et al.* 2011, Jha *et al.* 2013, Alijani and Amabili 2014). Many researchers investigated the flexural behaviour of FGM plates and shell panels using different equivalent single-layer theories.

Ma and Wang (2003) analyzed nonlinear bending behavior of FGM circular plates using classical von Karman strains and shooting method. Yang and Shen (2003) investigated nonlinear bending responses of FGM plates using higher-order shear deformation theory (HSDT) kinematics. Zhao *et al.* (2009) computed deflection and frequency responses of FGM cylindrical panel by adopting Ritz method. Santos *et al.* (2009) investigated the thermoelastic behavior of FGM cylindrical shell under thermal shocks using finite element method (FEM). Shen and Wang (2010) examined nonlinear bending analysis of FGM plate using HSDT kinematics. Singh and Talha (2010) analyzed the dynamic and free vibration characteristics of FGM plate via HSDT kinematics. Brischetto and Carrera (2010) investigated bending analysis of FGM structure using advanced mixed theories. Mantari (2011) presented deformation characteristics of functionally graded plates using HSDT kinematics. Mechab *et al.* (2012) studied static and dyanamic analysis of functionally graded plates using four variable refined plate theory. Thai and Choi (2013) studied about bending and vibration analysis of functionally graded plates using first-order shear deformation theory (FSDT). Valizadeh et al (2013) analyzed bending, vibration, buckling analysis of functionally graded materials using FSDT kinematics. Shen (2014) analyzed nonlinear thermal bending of FGM cylindrical panels using HSDT kinematics. Belabed *et al.* (2014) studied flexural behavior of of FGM plates using HSDT and normal theory. Zhang *et al.* (2015) analyzed nonlinear bending analysis of FGM circular plates via HSDT kinematics. Bellifa *et al.* (2015) analyzed nonlinear bending response of FGM circular plates based on physical neutral surface and HSDT. Yang *et al.* (2018) investigated bending analysis of 2D FGM nanobeams. Vu *et al.* (2017) examined bending and free vibration responses of FGM plates using first-order shear deformation theory (FSDT) in conjunction with finite element and mess-free methods. She *et al.* (2018) investigated the nonlinear bending of FGM porous tubes using nonlocal strain gradient theory. Babei *et al.* (2019) reported dynamic behavior of long cylindrical FGM panels using HSDT and Donnell's kinematics. Huang *et al.* (2020) analyzed bending and free vibration analysis of in-plane FGM plates using by high-order Chebyshev expansions combining with Gauss-Lobatto sampling. Mudhaffar *et al.* (2021) analyzed thermo mechanical bending behavior of FGM plate using HSDT. Bouafia *et al.* (2021) studied the bending and free vibration behavior of FGM Plates using quasi 3D-HSDT. Zaitoun *et al.* (2022) presented the buckling responses of FGM sandwich plate using HSDT. Tahir *et al.* (2021) analyzed wave propagation analysis of porous FGM sandwich plate using Hamilton principle. Bakoura *et al.* (2021) presented buckling analysis of FGM plates through HSDT.

In continuation to the above, very few attempts have been made by the researchers in past to analysis FGM structures with single/multiple cutouts. Fazilati and Ovesy (2013) investigated dynamic instability of longitudinal stiffened panel with rectangular internal cutouts using finite strip method. Yin *et al.* (2015) adopted simple and effective isogeometric analysis for buckling and

free vibration responses of thin laminated composite plates with cut-outs using NURBS basis function. Mehrparvar and Ghannadpour (2018) analyzed the nonlinear behavior of FGM plates contains rectangular holes via Ritz method. Zhong *et al.* (2021) studied thermal bending and vibration of FGM plates with various cutouts and complex shapes using isogeometric method.

It is noted from the above literature that most of the earlier works have been carried out on the deformation behaviour of FGM panels without intruding perforations. Based on the authors' knowledge, no work has been reported yet on thermoelastic deformation behavior of FGM cylindrical panels with single and multiple perforations. Here, the FGM constituents are considered to be temperature-dependent and the overall material properties are evaluated using Voigt's homogenisation scheme via power-law function. During the computations, different perforated structures with single (1×1) and multiple (2×2, 3×3 and 4×4) perforations are considered. Finally, the influence of various geometrical, material and loading parameters on deformation behaviour of perforated FGM cylindrical panel are exhibited through numerous examples and discussed in later section.

2. Overall material properties of FGM

In this analysis, metal/ceramic FGM is assumed in which elastic and thermal properties vary from metal-rich bottom surface to ceramic-rich top surface along thickness direction. Here, FGM ingredients are assumed to be temperature-dependent (Reddy and Chin 2007), as

$$\chi_{c,m}(T) = \chi_0(\chi_{-1}T^{-1} + 1 + \chi_1 T + \chi_2 T^2 + \chi_3 T^3) \tag{1}$$

where, T is elevated temperature. $\chi_{c,m}$ represents material properties of metal (m) and ceramic (c). $\chi_0, \chi_{-1}, \chi_1, \chi_2, \chi_3$ are the material constants.

Through-the-thickness gradation of FGM ingredients from bottom to top surfaces are achieved by adopting power-law function (Praveen and Reddy 1998), as

$$\left.\begin{aligned} \mu_c &= \left(\frac{z}{h} + \frac{1}{2}\right)^n \\ \mu_m &= 1 - \left(\frac{z}{h} + \frac{1}{2}\right)^n \end{aligned}\right\} \begin{matrix} -\frac{h}{2} \le z \le -\frac{h}{2} \\ 0 \le n < \infty \end{matrix} \tag{2}$$

where, n denotes power-law index, and h represents panel thickness. The variation of volume fraction of ceramic material along the thickness direction for different values of power-law index is illustrated in Fig. 1.

Now, the overall material properties of FGM (χ_{FGM}) can be computed using Voigt's micromechanical material scheme (Gibson *et al.* 1995), as

$$\chi_{FGM}(T,z) = \left(\chi_c(T) - \chi_m(T)\right)\left(\frac{z}{h} + \frac{1}{2}\right)^n + \chi_m(T) \tag{3}$$

Here, Eq. (3) can be utilised to evaluate Poisson's ratio (υ), modulus of elasticity (E) and coefficient of thermal expansion (α).

2.1 Geometrical description of perforated FGM cylindrical panel

In this study, FGM cylindrical panel of radius of curvature R and uniform thickness 'h' are considered in rectangular (a×b) planform with single (1×1) and/or multiple (2×2, 3×3 and 4×4)

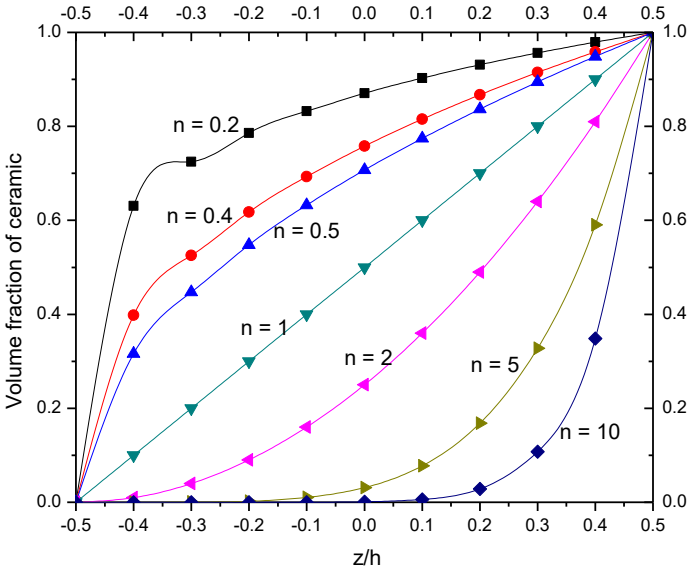

Fig. 1 Variation of volume fraction through the thickness

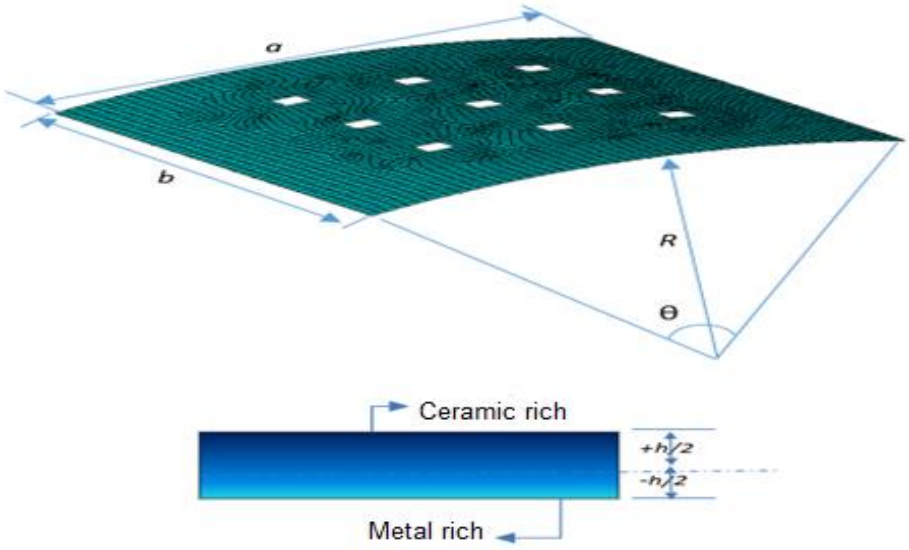

Fig. 2 Representation of FGM cylindrical shell panel with multiple perforations

perforations, as shown in Fig. 2 Here, all the cut-outs are rectangular ($c \times d$) and equispaced.

2.2 2D isoparametric finite element modelling

The kinematics of the present model is based on FSDT mid-plane with five degrees-of-freedom. The global displacements $(\bar{u}_1, \bar{u}_2, \bar{u}_3)$ at any point within the perforated FGM cylindrical panel are defined as

$$\left.\begin{aligned}\bar{u}_1(\bar{x},\bar{y},\bar{z}) &= u_1(\bar{x},\bar{y}) + z\phi_1(\bar{x},\bar{y})\\ \bar{u}_2(\bar{x},\bar{y},\bar{z}) &= u_2(\bar{x},\bar{y}) + z\phi_2(\bar{x},\bar{y})\\ \bar{u}_3(\bar{x},\bar{y},\bar{z}) &= u_3(\bar{x},\bar{y})\end{aligned}\right\} \tag{4}$$

where, (u_1, u_2, u_3) and (ϕ_1, ϕ_2) are the mid-plane displacement and rotation terms, respectively.

The strain tensor for the FG cylindrical panel can be written, as

$$\{\varepsilon\} = \begin{Bmatrix}\varepsilon_{xx}\\ \varepsilon_{yy}\\ \varepsilon_{xy}\\ \varepsilon_{xz}\\ \varepsilon_{yz}\end{Bmatrix} = \begin{Bmatrix}\frac{\partial \bar{u}_1}{\partial x} + \frac{\bar{u}_1}{R}\\ \frac{\partial \bar{u}_2}{\partial y}\\ \frac{1}{2}\left(\frac{\partial \bar{u}_1}{\partial y} + \frac{\partial \bar{u}_2}{\partial x}\right)\\ \frac{1}{2}\left(\frac{\partial \bar{u}_1}{\partial z} + \frac{\partial \bar{u}_3}{\partial x} - \frac{\bar{u}_1}{R}\right)\\ \frac{1}{2}\left(\frac{\partial \bar{u}_2}{\partial y} + \frac{\partial \bar{u}_3}{\partial x}\right)\end{Bmatrix} = \begin{Bmatrix}\varepsilon^0_{xx}\\ \varepsilon^0_{yy}\\ \varepsilon^0_{xy}\\ \varepsilon^0_{xz}\\ \varepsilon^0_{yz}\end{Bmatrix} + z\begin{Bmatrix}k^1_{xx}\\ k^1_{yy}\\ k^1_{xy}\\ k^1_{xz}\\ k^1_{yz}\end{Bmatrix} \tag{5}$$

Here, strain terms having superscripts 0 and 1 are membrane and flexural strains, res-pectively.

Eq. (5) can be rewritten in terms of mid-plane strain vector, as

$$\{\varepsilon\} = [H]\{\bar{\varepsilon}\} \tag{6}$$

Where, $[H]$ contains thickness coordinates.

The stress-strain relation of the perforated cylindrical FGM panel can be presented as

$$\sigma = C(\varepsilon_M - \varepsilon_T) \tag{7}$$

$$\begin{Bmatrix}\sigma_{xx}\\ \sigma_{yy}\\ \sigma_{xy}\\ \sigma_{yz}\\ \sigma_{xz}\end{Bmatrix} = \begin{bmatrix}\frac{E(T,z)}{1-v^2(T,z)} & \frac{v(T,z)E(T,z)}{1-v^2(T,z)} & 0 & 0 & 0\\ \frac{v(T,z)E(T,z)}{1-v^2(T,z)} & \frac{E(T,z)}{1-v^2(T,z)} & 0 & 0 & 0\\ 0 & 0 & \frac{E(T,z)}{2(1+v(T,z))} & 0 & 0\\ 0 & 0 & 0 & \frac{E(T,z)}{2(1+v(T,z))} & 0\\ 0 & 0 & 0 & 0 & \frac{E(T,z)}{2(1+v(T,z))}\end{bmatrix}\left(\begin{Bmatrix}\varepsilon_{xx}\\ \varepsilon_{yy}\\ \varepsilon_{xy}\\ \varepsilon_{yz}\\ \varepsilon_{xz}\end{Bmatrix} - \begin{Bmatrix}\alpha\Delta T\\ \alpha\Delta T\\ 0\\ 0\\ 0\end{Bmatrix}\right) \tag{8}$$

where [C] is the reduced stiffness matrix and $\Delta T$is the uniform temperature rise.

The governing equation of perforated FGM panel can be derived through principle of virtual work as

$$\delta W_\varepsilon = \delta W_{p+\Delta T} \tag{9}$$

Here, δW_ε is the total internal virtual work and is expressed as

$$\delta W_\varepsilon = \int_\Omega (\delta\varepsilon^T R\varepsilon) d\Omega \tag{10}$$

The external virtual work (δW_f) due to the transverse uniform load of intensity 'q' and temperature rise ΔT, can be expressed as

$$\delta W_{q+\Delta T} = \int \{\delta\lambda_o\}^T \{q\} dA + \int \{\delta\bar{\varepsilon}\}^T [C]\{\varepsilon_{th}\} dA \tag{11}$$

Here, eight noded quadrilateral elements are employed for discretization purpose with five

degrees of freedom per node. The field displacements are expressed in form of nodal displacements using shape functions (N_i), as

$$\lambda = \sum_{i=1}^{NNE=8} N_i \lambda_i \tag{12}$$

where, $\lambda_i = \{u_1 \ u_2 \ u_3 \ \phi_1 \ \phi_2\}_i^T$. The shape functions of eight noded quadrilateral element in ξ, η coordinates can be seen in Praveen and Reddy (2007). The strain vector can be presented in terms of nodal displacement vector as

$$\{\bar{\varepsilon}\} = [\partial]\{\lambda\} \tag{13}$$

where, $[\partial]$ is the differential operator matrix.

The internal virtual work over an element Ω_e using finite element formulation can be written as

$$(\delta W_\varepsilon)_e = \int_{\Omega^e} \{\delta\lambda_i\}_e^T [B_i]^T [S][B_i]\{\delta\lambda_i\}_e \{\delta\lambda_i\}_e d\Omega_e = \{\delta\lambda_i\}_e^T [K]_e \{\lambda_i\}_e$$

$$[S] = \begin{bmatrix} A_{11}A_{12}A_{16}B_{11}B_{12}B_{16}00 \\ A_{11}A_{22}A_{26}B_{12}B_{22}B_{26}00 \\ A_{16}A_{26}A_{66}B_{16}B_{26}B_{66}00 \\ B_{11}B_{12}B_{16}D_{11}D_{12}D_{16}00 \\ B_{12}B_{12}A_{16}D_{12}D_{22}B_{26}00 \\ B_{16}B_{22}A_{16}D_{16}D_{26}B_{66}00 \\ 00000000 \\ 00000000 \end{bmatrix} = \begin{bmatrix} AB0 \\ BD0 \\ 00A_S \end{bmatrix}$$

$$(A_{ij}, B_{ij}, D_{ij}) = \int_{\frac{-h}{2}}^{\frac{h}{2}} C_{ij}(1, z, z^2)\, dz; A_{s_{ij}} = k \int_{\frac{-h}{2}}^{\frac{h}{2}} C_{ij}\, dz \tag{14}$$

Here, *A*, *B*, *D* and A_s represent the extensional, coupling, bending, and transverse shear stiffness, respectively. However, *k* represents the transverse shear correction coefficient which is taken as same as in (Efraim and Eisenberger 2006).

$[K]^e$ is the element stiffness matrix which is evaluated numerically using full Gauss quadrature integration rule, as

$$[K]_e = \int_{\Omega_e} [B_i]^T [S][B_i] d\Omega_e = \int_{-1}^{1}\int_{-1}^{1} [B]^T [S][B] J d\xi dn = \sum_i^{g_i}\sum_j^{g_j} \left(\Phi_i \Phi_j J [B]^T [S][B]\right) \tag{15}$$

where, $[B]$ is the strain-displacement matrix which comprises different operators and shape functions.(Φ_i, Φ_j),(g_i, g_j) and *J* are the weigh factors, number of Gauss points and determinant of Jacobian matrix, respectively.

The external virtual work for an element$\Omega_e$due to uniform load (q) and temperature rise ΔT can be expressed, as

$$\left(\delta W_{q+\Delta T}\right)_e = \{\delta\lambda_i\}_e^T \left(\{F_{\Delta T}\}_e + \{F_q\}_e\right) \tag{16}$$

Here, $\{F_{\Delta T}\}_e$ and $\{F_q\}_e$ denote the elemental thermal and mechanical load vectors, respectively. Finally, the equilibrium equation of perforated FG cylindrical panel subjected to thermomechanical loadings can be governed by invoking principle of virtual work, as

$$[K]_e\{\lambda\}_e = \{F_{\Delta T}\}_e + \{F_q\}_e \tag{17}$$

Eq. (17) is further utilized for obtaining the system equations and solved via appropriate finite

Table 1 Properties of the metal and ceramic of FGM Constituents (Reddy and Chin 2007)

Materials	Properties					
	Property	T-1	T_0	T_1	T_2	T_3
Ti-6Al-4V	$E(Pa)$	0	1.225×1011	-4.586×10-04	0	0
	v	0	0.28	0	1.121×10-04	0
	$\alpha(k^{-1})$	0	7.5788×10-06	6.638×10-04	-3.147×10-06	0
Si3N4	$E(Pa)$	0	3.484×1011	-3.07×10-4	2.16×10-7	-8.946×10-11
	v	0	0.24	0	0	0
	$\alpha(k^{-1})$	0	5.872×10-6	9.095×10-4	0	0

Table 2 Mess sensitivity of FGM cylindrical panel with single/multiple perforations

Number of elements	1×1	Number of elements	2×2	Number of elements	3×3	Number of elements	4×4
17	0.007291	61	0.007265	119	0.007214	232	0.007263
42	0.00727	84	0.007268	173	0.007276	249	0.007297
81	0.00727	120	0.007284	198	0.007289	279	0.007314
171	0.007232	189	0.00731	282	0.007297	403	0.007317
554	0.007203	423	0.00729	416	0.007291	544	0.007318
768	0.007217	705	0.007287	833	0.007274	708	0.007321
1290	0.007198	1147	0.007264	1037	0.007274	1300	0.007301
1987	0.007193	1894	0.007266	2540	0.007249	1851	0.007299

element scheme to compute the desired flexural responses at various load steps.

3. Results and discussion

The deformation behaviour of FG cylindrical panels with single (1×1) and multiple (2×2, 3×3, 4×4) perforations are examined at various parameters to demonstrate the robustness of the developed model. In this section, silicon nitride (Si_3N_4) and titanium alloy (Ti-6Al-4V) are used as ceramic and metal materials, respectively and their properties are mentioned in Table 1. To reduce cost of computing and time conduct mesh sensitivity study on FEM related design and analysis.it helps to produce more reliable result and improve decision making for quality development cycle, mess sensitivity details are mentioned in Table 2.

For computational purpose, the perforated FG cylindrical panel are computed under clamed free (CFFF) support condition, as: $u_1 = u_2 = w_3 = \phi_1 = \phi_2 = 0$ at x=0. Also, the non-dimensional parameters are adopted for maximum deflection ($\bar{w} = w/h$) and uniformly distributed load ($p_o = p/E_m h^4$). Firstly, to check the effectiveness of present model, FG (Al/ZrO_2) cylindrical panels (a/h=20, *CFCF* and R/a=5) are analysed at different power-law indices (n=0, 0.2, 0.5, 1, 2) as in Table 3. Here, the material properties parameters are taken as same as in Zhao *et al.* (2009). It shows the deviation between the present results and the results of Zhao *et al.* (2009) are very nominal, i.e., ≤1.2%.

Table 3 Validation of Non-dimensional maximum deflections of CFCF square (Al/ZrO_2) cylindrical panel

Power-law index (n)	Present	(Zhao *et al.* 2009)	% difference
0	0.027609	0.02778	-0.6193
0.2	0.031206	0.0313	-0.3012
0.5	0.034998	0.03535	-1.0057
1	0.039097	0.03956	-1.1842
2	0.043038	0.04333	-0.6784

Table 4 Contour plot of functionally graded cylindrical panels with multiple perforations at different temperature

Temperature	1×1 Perforation	2×2 Perforation	3×3 Perforation	4×4 Perforation
300K	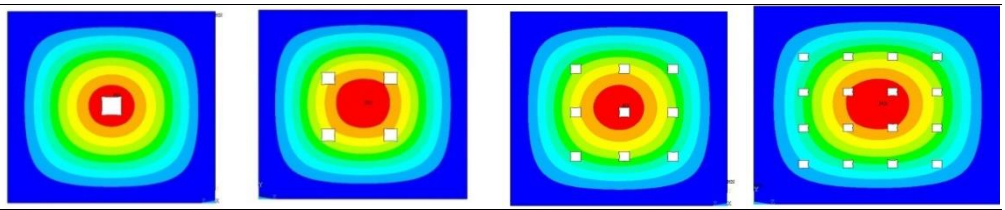			
400K	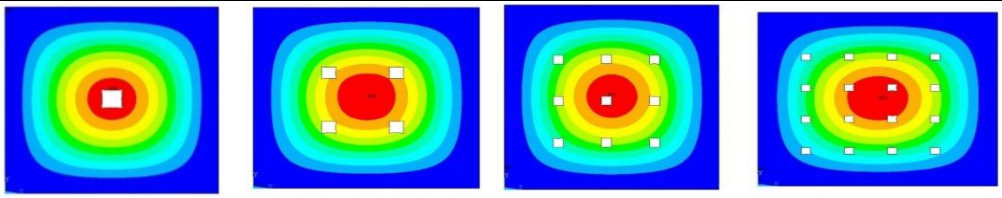			
500K	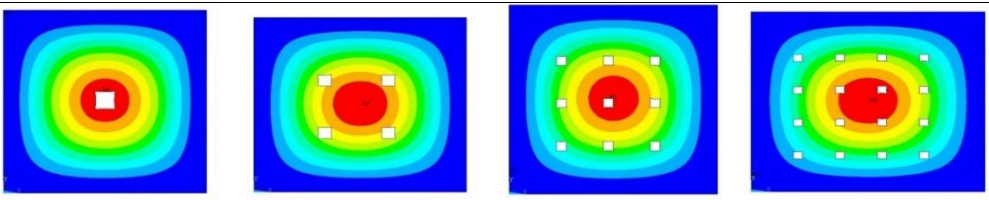			
600K	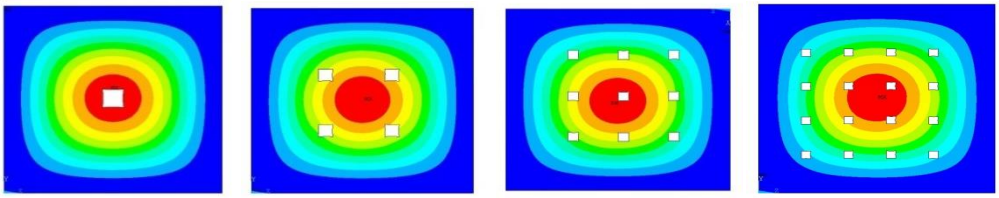			
700K	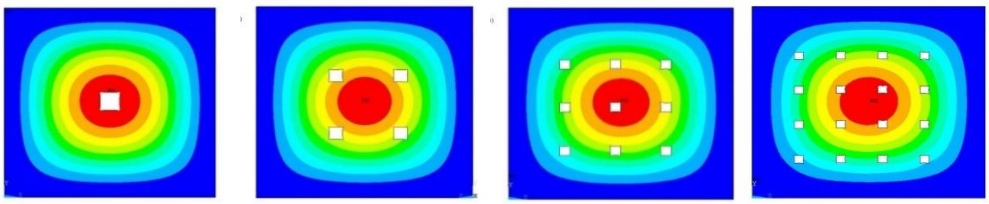			

Contour plots display the results of a single data set over the model geometry. The range of values in the results set is divided into a number of subrange, and each subrange is assigned a

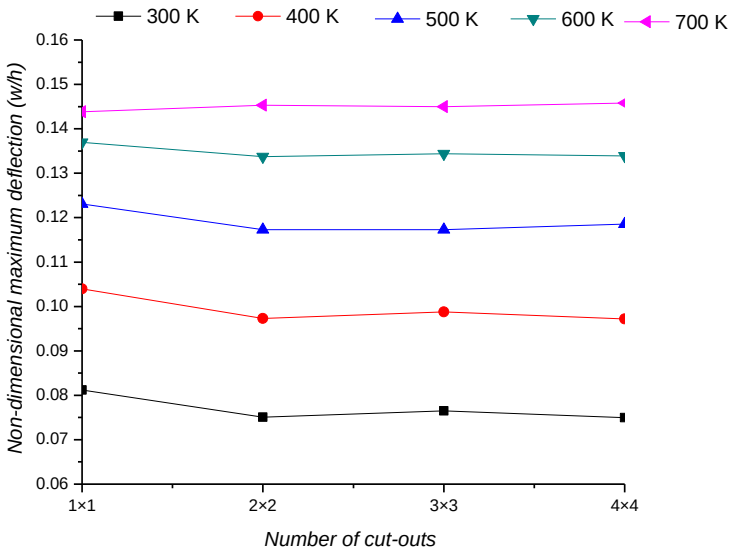

Fig. 3 Variation of non-dimensional maximum deflection of perforated FG (Si3N4/ Ti-6Al-4V) cylindrical (a/h=20, a/b=1, n=0.5) panels at various temperature

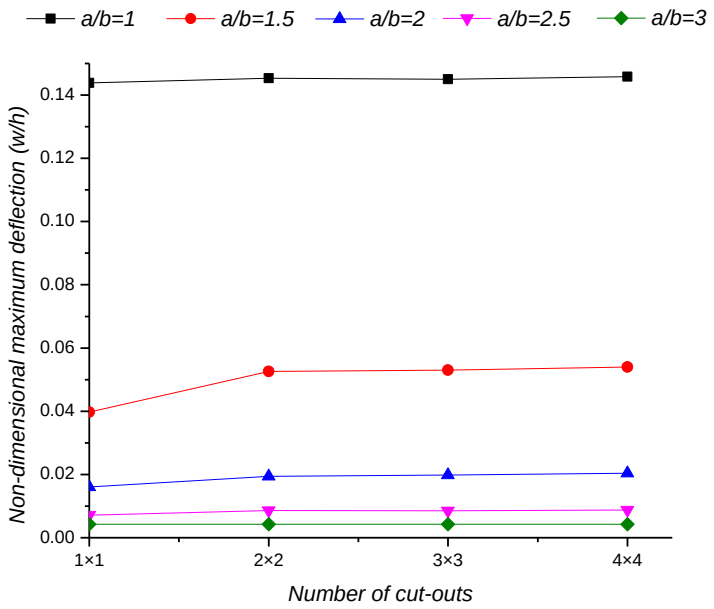

Fig. 4 Variation of non-dimensional maximum deflection of perforated FG (Si_3N_4/ Ti-6Al-4V) cylindrical (a/h=20, T=700, n=0.5) panels at various aspect ratios

colour shown in Table 4.

Fig. 3 shows the non-dimensional maximum deflections of moderately thick (b/h=20, CFFF, a/b=1, n=0.5, r=5) perforated (1×1, 2×2, 3×3, 4×4) FG cylindrical panels under different temperatures. It is observed that the non-dimensional deflections increase with the temperature rise from 300 K to 700 K because stiffness of the structure reduces with the temperature rise. In

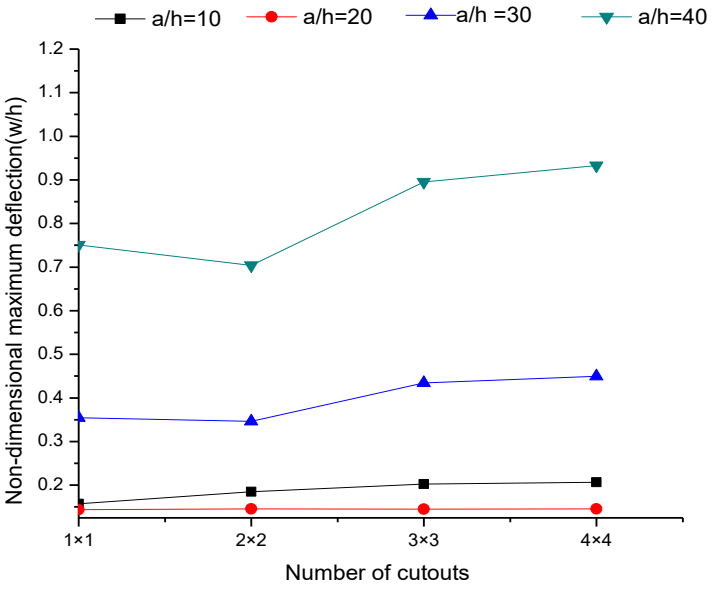

Fig. 5 Variation of non-dimensional maximum deflection of FG (Si_3N_4/Ti-6Al-4V) cylindrical (T=700 K, a/b=1, n=0.5) panel at different thickness ratios

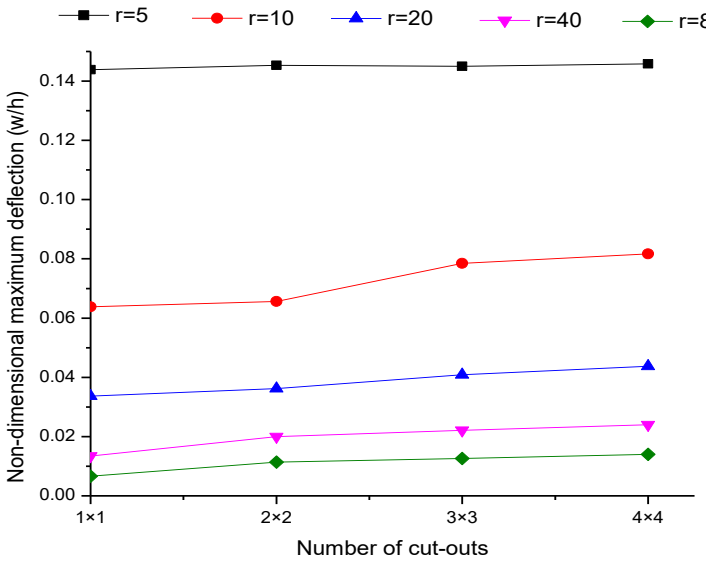

Fig. 6 Variation of non-dimensional maximum deflection of FG (Si_3N_4/Ti-6Al-4V) cylindrical (T=700, a/b=1, n=0.5, a/h=20) panel at different curvature ratios

addition to this, the maximum deflection responses at 700 K are almost twice of the responses at 300 K. From temperature rise 300 K to 600 K, FG cylindrical panels with single cutout (1×1) exhibit highest deflection values whereas; perforated (4×4) FG cylindrical panel demonstrates the highest response value at 700 K. This mix-type of behaviour is observed because the surface area of the FG cylindrical panels with single/multiple perforations are kept constant.

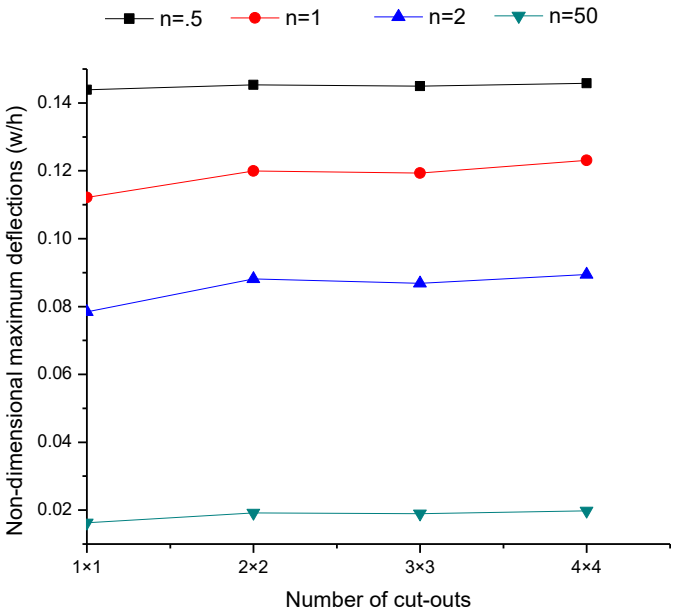

Fig. 7 Variation of non-dimensional maximum deflection of FG (Si_3N_4/Ti-6Al-4V) cylindrical (*a*/*h*=20, *T*=700 K, *a*/*b*=1) panel at different power-law indices.

Fig. 4 shows the non-dimensional maximum deflections of moderately thick (*b*/*h*=20, CFFF, *n*=.5, *r*=5, *T*=700K) perforated (1×1, 2×2, 3×3, 4×4) FG cylindrical panels at different aspect ratios (*a*/*b*=1, 1.5, 2, 2.5, 3). The non-dimensional deflection responses are reducing rapidly by enhancing the aspect ratios from *a*/*b*=1 to *a*/*b*=1.5, and then gradually upto *a*/*b*=3. Also, FG cylindrical panel with single cutout (1×1) exhibits the lowest deflection whereas perforated (4×4) FG cylindrical panel has highest deflection values. It is also noted that aspect ratio of panel and cutout are identical.

Fig. 5 shows the non-dimensional maximum deflections of (CFFF, *a*/*b*=1, *n*=.5, *r*=5, *T*=700K) perforated (1×1, 2×2, 3×3, 4×4) FG cylindrical panels at different thickness ratios (*b*/*h*=10, 20, 30, 40). Here, deflection parameters show the non-monotonous behaviour with respect to thickness ratios. However, the significance of number of perforations in moderately thick perforated FG cylindrical panels are almost nominal. In all the cases, perforated (4×4) FG cylindrical panel demonstrates highest deflection response.

Fig. 6 shows the non-dimensional maximum deflections of moderately thick (*b*/*h*=20, CFFF, *a*/*b*=1, *n*=.5, *T*=700K) perforated (1×1, 2×2, 3×3, 4×4) FG cylindrical panels at different curvature ratios (*r*=5,10, 20, 40, 80). It is observed that the deflection responses decrease as increases of curvature ratios, whereas, the deflection responses are maximum in perforation (4×4) and minimum in (1×1).

Fig. 7 shows the non-dimensional maximum deflections of moderately thick (*b*/*h*=20, CFFF, *a*/*b*=1, *r*=5, *T*=700K) perforated (1×1, 2×2, 3×3, 4×4) FG cylindrical panels at different power-law indices (*n*=0.5, 1, 2, 50). It is analysed that the non-dimensional deflection decreases as the power-law index increases. In all the consider cases, perforated FG cylindrical panel demonstrates very small changes of perforation effect on FGM cylindrical panel.

4. Conclusions

The deformation responses of perforated FG cylindrical panel are examined under thermo-mechanical loading. Here, single and multiple cutouts (1×1, 2×2, 3×3, 4×4) are considered in panels without altering the surface area. The material properties of perforated FG panels are graded in the thickness direction according to Voigt's micromechanical material scheme via power-law function. The final responses are obtained using the 2D-isoparametric finite element approximations via eight-noded quadrilateral elements. The validation and comparison studies have been made with the reported literature. The efficiency of the developed model has been checked by computing the deflection responses at various sets of parametric combinations. The numerical illustrations reveal the significance of the present analysis, as non-monotonous behavior of deflection responses are confirmed for perforated (1×1, 2×2, 3×3, 4×4) FG cylindrical panels at various sets of conditions. However, in most of the cases, perforated (4×4) FG cylindrical panel demonstrates highest deflection.

Acknowledgement

The authors would like to thank Science and Engineering Research Board, Department of Science and Technology, Government of India (File No. ECR/2016/001829) for the financial support.

References

Alijani, F. and Amabili, M. (2014), "Non-linear vibrations of shells: A literature review from 2003 to 2013", *Int. J. Nonlin. Mech.*, **58**, 233-257. https://doi.org/10.1016/j.ijnonlinmec.2013.09.012.

Babaei, H., Kiani, Y. and Eslami, M.R. (2019), "Large amplitude free vibrations of long FGM cylindrical panels on nonlinear elastic foundation based on physical neutral surface", *Compos. Struct.*, **220**, 888-898. https://doi.org/10.1016/j.compstruct.2019.03.064.

Bakoura, A., Bourada, F., Bousahla, A.A., Tounsi, A., Benrahou, K.H., Tounsi, A., ... & Mahmoud, S.R. (2021), "Buckling analysis of functionally graded plates using HSDT in conjunction with the stress function method", *Comput. Concrete*, **27**, 1598-9198. https://doi.org/10.12989/cac.2021.27.1.073.

Belabed, Z., Houari, M.S.A., Tounsi, A., Mahmoud, S.R. and Bég, O.A. (2014), "An efficient and simple higher order shear and normal deformation theory for functionally graded material (FGM) plates", *Compos.: Part B*, **60**, 274-283. https://doi.org/10.1016/j.compositesb.2013.12.057.

Bellifa, H., Benrahou, K.H., Hadji, L., Houari, M.S.A. and Tounsi, A. (2015), "Bending and free vibration analysis of functionally graded plates using a simple shear deformation theory and the concept the neutral surface position", *J. Brazil. Soc. Mech. Sci. Eng.*, **38**(1), 265-275. https://doi.org/10.1007/s40430-015-0354-0.

Birman, V. and Byrd, L.W. (2007), "Modeling and analysis of functionally graded materials and structures", *Appl. Mech. Rev.*, **60**, 195-216. https://doi.org/10.1115/1.2777164.

Bouafia, K., Selim, M.M., Bourada, F., Bousahla, A.A., Bourada, M., Tounsi, A., ... & Tounsi, A. (2021), "Bending and free vibration characteristics of various compositions of FG plates on elastic foundation via quasi 3D HSDT model". *Steel Compos. Struct.*, **41**, 487-503. https://doi.org/10.12989/scs.2021.41.4.487.

Brischetto, S. and Carrera, E. (2010), "Advanced mixed theroies for bending analysis of functionally graded plates", *Comput. Struct.*, **88**, 1474-1483. https://doi.org/10.1016/j.compstruc.2008.04.004.

Efraim, E. and Eisenberger, M (2006), "Exact vibration analysis of variable thickness thick annular isotropic

and FGM plates", *J. Sound Vib.*, **299**, 720-738. https://doi.org/10.1016/j.jsv.2006.06.068.
Fazilati, J. and Ovesy, H.R. (2013), "Parametric instability of laminated longitudinally stiffened curved panels with cutout using higher order FSM", *Compos. Struct.*, **95**, 691-696. https://doi.org/10.1016/j.compstruct.2012.08.034.
Gibson, L.J., Ashby, M.F., Karam, G.N., Wegst, U. and Shercliff, H.R. (2005), "Mechanical properties of natural materials. II. Microstructures for mechanical efficiency", *Proc. Roy. Soc. London Ser. A*, **450**, 141-162. https://doi.org/10.1098/rspa.1995.0076.
Huang, Y., Zhao, Y. and Cao, D. (2020), "Bending and free vibration analysis of orthotropic in- plane functionally graded plates using a Chebyshev spectral approach", *Compos. Struct.*, **255**, 112938. https://doi.org/10.1016/j.compstruct.2020.112938.
Jha, D.K., Kant, T. and Singh, R.K. (2013), "A critical review of recent research on functionally graded plates", *Compos. Struct*., **96**, 833-849. http://doi.org/10.1016/j.compstruct.2012.09.001.
Liew, K.M. (1993), "On the use of pb-2 Rayleigh-Ritz method for free-flexural vibration of triangular plates with curved internal supports", *J. Sound Vib.*, **165**, 329-340. https://doi.org/10.1006/jsvi.1993.1260.
Liew, K.M., Zhao, X. and Ferreira, A.J.M. (2011), "A review of meshless methods for laminated and functionally graded plates and shells", *Compos. Struct.*, **93**(8), 2031-2041. https://doi.org/10.1016/j.compstruct.2011.02.018.
Ma, L.S. and Wang, T.J. (2003), "Nonlinear bending and post-buckling of a functionally graded circular plate under mechanical and thermal loadings", *Int. J. Solid. Struct.*, **40**, 3311-3330. https://doi.org/10.1016/S0020-7683(03)00118-5.
Mantari, J.L., Oktem, A.S. and Soares, C.G. (2011), "Bending response of functionally graded plates by using a new higher order shear deformation theory", *Compos. Struct.*, **94**, 714-723. https://doi.org/10.1016/j.compstruct.2011.09.007.
Mechab, I., Mechab, B. and Benaissa, S. (2012), "Static and dynamic analysis of functionally graded plates using Four-variable refined plate theory by the new function", *Compos.: Part B*, **45**, 748-757. https://doi.org/10.1016/j.compositesb.2012.07.015.
Mehrparvar, M. and Ghannadpour, S.A.M. (2018), "Plate assembly technique for nonlinear analysis of relatively thick functionally graded plates containing rectangular holes subjected to in-plane compressive load", *Compos. Struct.*, **202**, 867-880. https://doi.org/10.1016/j.compstruct.2018.04.053.
Mudhaffar, I.M., Tounsi, A., Chikh, A., Al-Osta, M.A., Al-Zahrani, M.M. and Al-Dulaijan, S.U. (2021), "Hygro-thermo-mechanical bending behavior of advanced functionally graded ceramic metal plate resting on a viscoelastic foundation", *Struct.*, **33**, 2177-2189. https://doi.org/10.1016/j.istruc.2021.05.090.
Praveen, G.N. and Reddy, J.N (1998), "Nonlinear transient thermoelastic analysis of functionally graded ceramic metal plates", *Int. J. Solid Struct*., **35**, 4457-4479. https://doi.org/10.1016/S0020-7683(97)00253-9.
Reddy, J.N and Chin, C.D (2007), "Thermomechanical analysis of functionally graded cylinders and plates", *J. Therm. Stress.*, **21**, 593-626. https://doi.org/10.1080/01495739808956165.
Santos, H., Soares, C.M.M., Soares, C.A.M. and Reddy, J.N. (2009), "A semi-analytical finite element model for the analysis of cylindrical shells made of functionally graded materials", *Compos. Struct.*, **91**, 427-432. https://doi.org/10.1016/j.compstruct.2009.04.008.
She, G.L., Yuan, F.G., Ren, Y.R., Liu, H.B. and Xiao, W.S. (2018), "Nonlinear bending and vibration analysis of functionally graded porous tubes via a nonlocal strain gradient theory", *Compos. Struct.*, ***203***, 614-623. https://doi.org/10.1016/j.compstruct.2018.07.063.
Shen, H.S. (2014), "Nonlinear thermal bending of FGM cylindrical panels resting on elastic foundations under heat conduction", *Compos. Struct.*, **113**, 216-224. https://doi.org/10.1016/j.compstruct.2014.03.034.
Tahir, S.I., Chikh, A., Tounsi, A., Al-Osta, M.A., Al-Dulaijan, S.U. and Al-Zahrani, M.M. (2021), "Wave propagation analysis of a ceramic-metal functionally graded sandwich plate with different porosity distributions in a hygro-thermal environment", *Compos. Struct.*, **269**, 114030. https://doi.org/10.1016/j.compstruct.2021.114030.
Talha, M. and Singh, B. (2010), "Static response free vibration analysis of FGM plates using high order shear deform theory", *Appl. Math. Model.*, **34**, 3991-4011. https://doi.org/10.1016/j.apm.2010.03.034.
Thai, H.T. and Choi, D.H. (2013), "A simple first-order shear deformation theory for the bending and free

vibration analysis of functionally graded plates", *Compos. Struct.*, **101**, 332-340. https://doi.org/10.1016/j.compstruct.2013.02.019.

Valizadeh, N., Natarajan, S., Gonzalez-Estrada, O.A., Rabczuk, T., Bui, T.Q. and Bordas, S.P. (2013), "NURBS-based finite element analysis of functionally graded plates: Static bending, vibration, buckling and flutter", *Compos. Struct.*, **99**, 309-326. https://doi.org/10.1016/j.compstruct.2012.11.008.

Vu, T.V., Nguyen, N.H., Khosravifard, A., Hematiyan, M.R., Tanaka, S. and Bui, T.Q. (2017), "A simple FSDT-based meshfree method for analysis of functionally graded plates", *Eng. Anal. Bound. Elem.*, **79**, 1-12. https://doi.org/10.1016/j.enganabound.2017.03.002.

Yang, J. and Shen, H.S (2003), "Nonlinear bending analysis of shear deformable functionally graded plates subjected to thermo-mechanical loads under various boundary conditions", *Compos.: Part B*, **34**, 103-115. https://doi.org/10.1016/S1359-8368(02)00083-5.

Yin, S., Yu, T., Bui, T.Q., Xia, S. and Hirose, S. (2015), "A cutout isogeometric analysis for thin laminated composite plates using level sets", *Compos. Struct.*, **127**, 152-164. https://doi.org/10.1016/j.compstruct.2015.03.016.

Zaitoun, M.W., Chikh, A., Tounsi, A., Al-Osta, M.A., Sharif, A., Al-Dulaijan, S.U. and Al-Zahrani, M.M. (2022), "Influence of the visco-Pasternak foundation parameters on the buckling behavior of a sandwich functional graded ceramic-metal plate in a hygrothermal environment", *Thin Wall. Struct.*, **170**, 108549. https://doi.org/10.1016/j.tws.2021.108549.

Zenkour, A.M. and Hafed, Z.S. (2020), "Bending response of functionally graded piezoelectric plates using a two-variable shear deformation theory", *Adv. Aircraft Spacecraft Sci.*, **7**(2), 115-134. https://doi.org/10.12989/aas.2020.7.2.115.

Zhang, D.G. and Zhou, H.M. (2015), "Nonlinear bending analysis of FGM circular plates based on physical neutral surface and higher-order shear deformation theory", *Aerosp. Sci. Technol.*, **41**, 90-98. https://doi.org/10.1016/j.ast.2014.12.016.

Zhao, X., Lee, Y.Y. and Liew, K.M. (2009), "Thermoelastic and vibration analysis of functionally graded cylindrical shells", *Int. J. Mech. Sci.*, **51**(9-10), 694-707. https://doi.org/10.1016/j.ijmecsci.2009.08.001.

Zhong, S., Zhang, J., Jin, G., Ye, T. and Song, X. (2021), "Thermal bending and vibration of FGM plates with various cutouts and complex shapes using isogeometric method", *Compos. Struct.*, **260**, 113518. https://doi.org/10.1016/j.compstruct.2020.113518.

GY